Journal of ELECTRONIC MATERIALS, Vol. 47, No. 2, 2018
DOI: 10.1007/s11664-017-5849-2
© 2017 The Minerals, Metals & Materials Society

TOPICAL COLLECTION: 59TH ELECTRONIC MATERIALS CONFERENCE 2017

Dependence of Internal Crystal Structures of InAs Nanowires on Electrical Characteristics of Field Effect Transistors

SANGMOON HAN,[1] ILGYU CHOI,[1] KWANJAE LEE,[1] CHEUL-RO LEE,[1] SEOUNG-KI LEE,[2] JEONGWOO HWANG,[3] DONG CHUL CHUNG,[4] and JIN SOO KIM[1,5]

1.—Division of Advanced Materials Engineering and Research Center of Advanced Materials Development, Chonbuk National University, Jeonju 54896, South Korea. 2.—Applied Quantum Composites Research Center, Korea Institute of Science and Technology, Wanju 55324, South Korea. 3.—Laser Research Center, Korea Photonics Technology Institute, Gwangju 61007, South Korea. 4.—Korea Institute of Carbon Convergence Technology, Jeonju 54853, South Korea. 5.—e-mail: kjinsoo@jbnu.ac.kr

We report on the dependence of internal crystal structures on the electrical properties of a catalyst-free and undoped InAs nanowire (NW) formed on a Si(111) substrate by metal–organic chemical vapor deposition. Cross-sectional transmission electron microscopy images, obtained from four different positions of a single InAs NW, indicated that the wurtzite (WZ) structure with stacking faults was observed mostly in the bottom region of the NW. Vertically along the InAs NW, the amount of stacking faults decreased and a zinc-blende (ZB) structure was observed. At the top of the NW, the ZB structure was prominently observed. The resistance and resistivity of the top region of the undoped InAs NW with the ZB structure were measured to be 121.5 kΩ and 0.19 Ω cm, respectively, which are smaller than those of the bottom region with the WZ structure, i.e., 251.8 kΩ and 0.39 Ω cm, respectively. The reduction in the resistance of the top region of the NW is attributed to the improvement in the crystal quality and the change in the ZB crystal structure. For a field effect transistor with an undoped InAs NW channel, the drain current versus drain–source voltage characteristic curves under various negative gate–source voltages were successfully observed at room temperature.

Key words: InAs, nanowire, structural properties, electrical properties, field-effect transistor

INTRODUCTION

In recent years, compound-semiconductor nanowires (NWs) have been actively studied with reference to their fundamental physics and potential device applications due to their unique electrical and optical properties.[1–4] In particular, InAs NWs have attracted considerable interest for applications in optoelectronic devices, such as terahertz emitters/detectors and transistors.[5–9] Typically, InAs NWs are fabricated using metallic catalysts, such as gold and nickel (Ni). However, metallic catalysts often create deep levels in the energy bandgap mainly due to chemical contamination.[5,10,11] This has the potential to degrade their electrical and optical properties. Wang et al.[11] reported that Au catalysts introduced deep-level traps in the semiconductor band gap, limiting the performances of functional Si-based optoelectronic devices. Recently, several research groups have reported catalyst-free or self-catalyst InAs NWs using vapor–liquid–solid or Volmer–Weber modes to reduce the chemical contamination caused by the metallic catalysts.[12–14] The catalyst-free InAs NWs were mostly fabricated

(Received July 4, 2017; accepted October 3, 2017; published online October 24, 2017)

on Si substrates.[1,15,16] However, because of the large difference in material parameters between InAs and Si, including lattice constants and thermal expansion coefficients, it is quite difficult to form InAs NWs with a high crystal quality; that is, catalyst-free InAs NWs on Si substrates showed many structural defects, including stacking faults.[17–19] In addition, two different crystal structures, zinc-blende (ZB) and wurtzite (WZ), are usually observed inside InAs NWs. The co-existence of both crystal structures inside the NWs significantly influences their electrical and optical properties.

Miao et al.[20] demonstrated InAs NW-based near-infrared photodetectors having a detection wavelength of up to ~ 1.5 μm and a small hysteresis width with a high on/off ratio. Cuil et al.[21] reported spintronic devices (Datta–Das spin transistor) with an InAs NW as the transport channel. Chen et al.[22] reported on the correlation of the electrical transport properties with the crystal phase and orientation of single-crystal InAs NWs used in field effect transistor (FET) channels. They showed that ZB and WZ crystal phases significantly influenced the band structure of InAs NWs resulting in performance variations of the device. Dayeh et al.[8] compared the contact resistance of an InAs NW grown on SiO_2/Si with that of a WZ-InAs NW formed on a boron substrate. The contact resistance of the ZB-InAs NW was 1.48 kΩ, which is smaller than that of the WZ NW. However, the dependence of internal crystal structures on the electrical properties of a single InAs NW with both ZB and WZ structures has yet to be studied. In addition, the low-temperature operation of a FET with the InAs NWs as the channel medium was reported.[6,23] Konar et al.[23] reported that the carrier transport in FETs with a NW channel was limited by the remote Coulomb scattering and acoustic phonon scattering at room temperature (RT). That is, it is quite difficult to measure the electrical characteristics of a FET with a single InAs NW at RT mainly because of the many stacking faults and carrier–phonon interactions that disturb the carrier movement.

In this paper, we discuss the effects of the internal ZB and WZ crystal structures on the electrical properties of a catalyst-free and undoped InAs NW formed on a Si substrate. Transmission-electron microscopy (TEM) images indicated that the ratio between WZ and ZB structures were differently observed depending on the position of the single InAs NW in the vertical direction. To investigate the electrical properties of the InAs NW with respect to their internal crystal structures, current–voltage (I–V) curves were measured at two different areas. The resistance and resistivity at the top region of the InAs NW were measured to be 121.5 kΩ and 0.19 Ω cm, respectively, which are smaller than those of the bottom area, i.e., 251.8 kΩ and 0.39 Ω cm, respectively. In addition, we fabricated a FET with an undoped InAs NW as a channel medium and investigated the drain current (I_D) versus the drain–source voltage (V_{DS}) at negative gate–source voltages (V_{GS}) ranging from 0 V to $-$ 20 V.

EXPERIMENTAL

InAs NWs were grown on a Si(111) substrate by Aixtron metal–organic chemical vapor deposition (MOCVD). Before InAs NW formation, the Si(111) substrate was chemically cleaned by a standard wet-etching process using acetone, methanol, isopropyl alcohol, and deionized water. After the chemical deoxidation process, the Si(111) substrate was immediately loaded into a MOCVD system. The MOCVD reactor was pumped down to a pressure of 50 mbar and heated to 570°C. After temperature stabilization, arsine (AsH_3) gas was flowed into the reactor for 1 min, and then trimethylindium (TMIn) gas was simultaneously supplied into the reactor for InAs NW growth. The molar flows of the AsH_3 and TMIn were 2.2×10^{-4} mol/min and 2.2×10^{-5} mol/min, respectively.

The as-grown InAs NWs were characterized using field-emission scanning electron microscopy (FE-SEM; Hitachi SU-70) and aberration-corrected TEM (Cs-TEM; JEOL JEM-ARM200F). Prior to electrical property investigation, the NWs were separated from the Si substrate by 1-min sonication in isopropanol to afford a diluted InAs NW solution. The InAs NWs were dispersed by dropping the diluted InAs NW solution onto a Si substrate covered by a SiO_2 layer with a thickness of 300 nm. Then, 80 nm-thick Ni electrodes were deposited on selected positions of a single InAs NW by using e-beam lithography and lift-off processing. For the fabrication of a FET with an InAs NW channel, source and drain terminals were formed by depositing Ni at two different positions separated by 5 μm.

RESULTS AND DISCUSSION

Figure 1a and b shows the cross-sectional and plan-view FE-SEM images, respectively, of catalyst-free InAs NWs formed on a Si(111) substrate. In Fig. 1a, chunk structures right above the Si substrate indicate that the InAs NWs were formed by the Volmer–Weber growth mode.[5,24] The average width of the InAs NWs was measured to be 293 nm. The lengths of the InAs NWs were distributed in the range from 8 μm to 18 μm. The external shape and width of each InAs NW were not significantly changed along the vertical direction. However, the relatively long InAs NWs were lightly bent near the top. As seen in Fig. 1b, the top surfaces of relatively short InAs NWs, marked as blue dotted circles, show a hexagonal shape, while the relatively long InAs NWs, denoted as a red circle, show a polygonal shape. The inset in Fig. 1b is a magnified image of a single InAs NW with the length of 15 μm, where the polygonal surface was clearly observed. That is, the surface is regularly rugged because of alternating

polar-type facets in the InAs NW with a ZB structure.[25,26] These two different surfaces correspond to the internal WZ and ZB crystal structures. That is, even if an InAs NW is grown on the same Si substrate, the crystal structures vary according to the position of InAs NWs.

Figure 2 shows the Cs-TEM image of a catalyst-free and undoped InAs NW with the length of 18 μm. The high-resolution TEM (HRTEM) and diffraction patterns, which were measured at four different positions of the NW along the vertical axis, are added in the right-hand side of the Cs-TEM image. The HRTEM images show that the stacking faults (alternate bright and dark features) were observed from all regions of the InAs NW. However, the upper region of the InAs NW corresponding to regions (I) and (II) has fewer stacking faults than the bottom areas denoted as regions (III) and (IV). The relatively large amount of stacking faults at the bottom area of the InAs NW can be attributed to the large lattice mismatch and difference in thermal expansion coefficients between InAs and Si substrate. For the bottom region of the InAs NW, the diffraction patterns are rather complex mainly due to irregularities of the crystalline structures of the WZ and the ZB, and the influence of stacking faults. Particularly for the region (IV), it is not easy to analyze the diffraction patterns. As marked by the black dotted circles, the WZ and ZB crystal structures are weakly confirmed from the diffraction patterns of $[01\bar{1}0]$ and [111], respectively. For region (III), the diffraction patterns are more clearly distinguished than those for region (IV), where the pattern information on the [0001] was newly monitored. Moving upwards to regions (I) and (II), the diffraction patterns of [111] and $[0\bar{2}\bar{2}]$ corresponding to the ZB structure are predominantly observed, because of the reduction in stacking faults in the WZ portion. Since the lattice constant of the ZB-InAs NW is similar to that of the WZ one, the difference in the total system energy caused by the lattice constant should be small between the two crystal structures. As a result, metastable multi-phase structures can be easily formed inside InAs NWs.[27–29] That is, the ZB and WZ structures are mixed up in the middle of an InAs NW. However, since the ZB structure for InAs is intrinsically more stable than the WZ structure, there is more ZB and less WZ structure in the NW along the vertical axis.

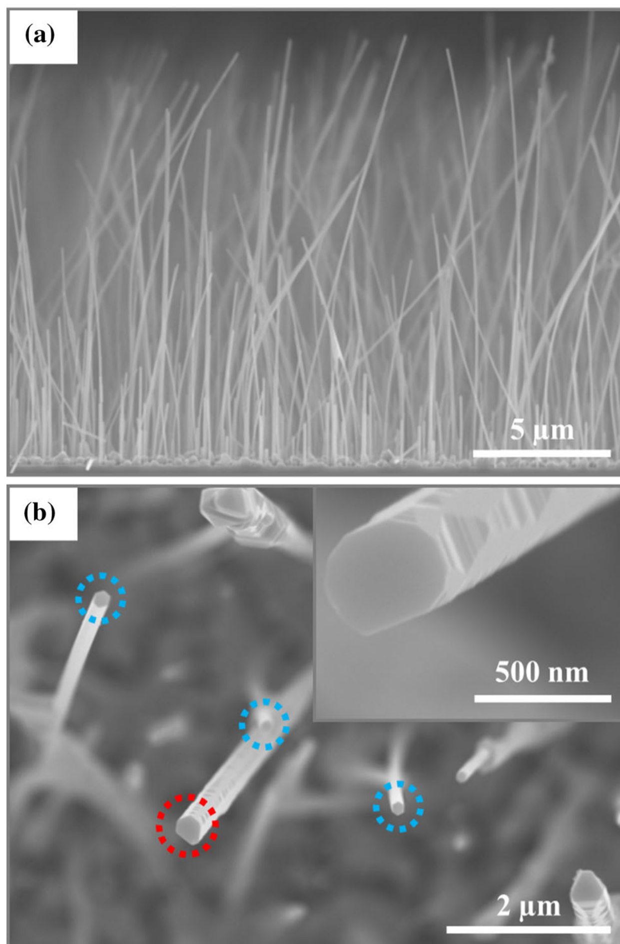

Fig. 1. (a) Cross-sectional and (b) plan-view FE-SEM images of InAs NWs. Inset a magnified image of a relatively long InAs NW.

Figure 3 shows the *I*–*V* characteristic curves of an undoped InAs NW, measured at the top and bottom regions. The inset is an optical microscopy (OM) image of an InAs NW-based device fabricated on a SiO_2/Si substrate. To study the electrical characteristics of the device, we deposited Ni as electrode material to form a quasi-Ohmic contact with the InAs NW.[30,31] The distance between two adjacent metal contacts is 5 μm. "Region-A" and "Region-B" correspond to the bottom and top regions of a single InAs NW, respectively. As described before, the crystalline structures of the WZ and the ZB co-exist with stacking faults at the bottom region of the InAs NW. Meanwhile, the ZB structure was dominantly observed with a reduced WZ structure and stacking faults at the top region. These kinds of structural properties certainly influence the electrical characteristics of the InAs NWs. The slope of the *I*–*V* characteristic curve for "Region-B" is steeper than that for "Region-A". The resistance and resistivity estimated from the *I*–*V* curve for "Region-B" corresponding to the top area of the undoped InAs NW were measured to be 121.5 kΩ and 0.19 Ω cm, respectively, which are smaller than those of "Region-A", 251.8 kΩ and 0.39 Ω cm, respectively. This can be attributed to the many stacking faults and the WZ structure in "Region-A" interfering with the carrier behavior when compared to the ZB structure. Since the inherent crystal structure of bulk InAs is ZB, resistance and resistivity for the ZB-InAs NW are lower than those for the WZ-InAs NWs. Generally, the WZ structure has non-zero spontaneous polarization resulting in the existence of an internal electric field.[12,32] Dayeh et al.[8] reported that polarization charges create negative

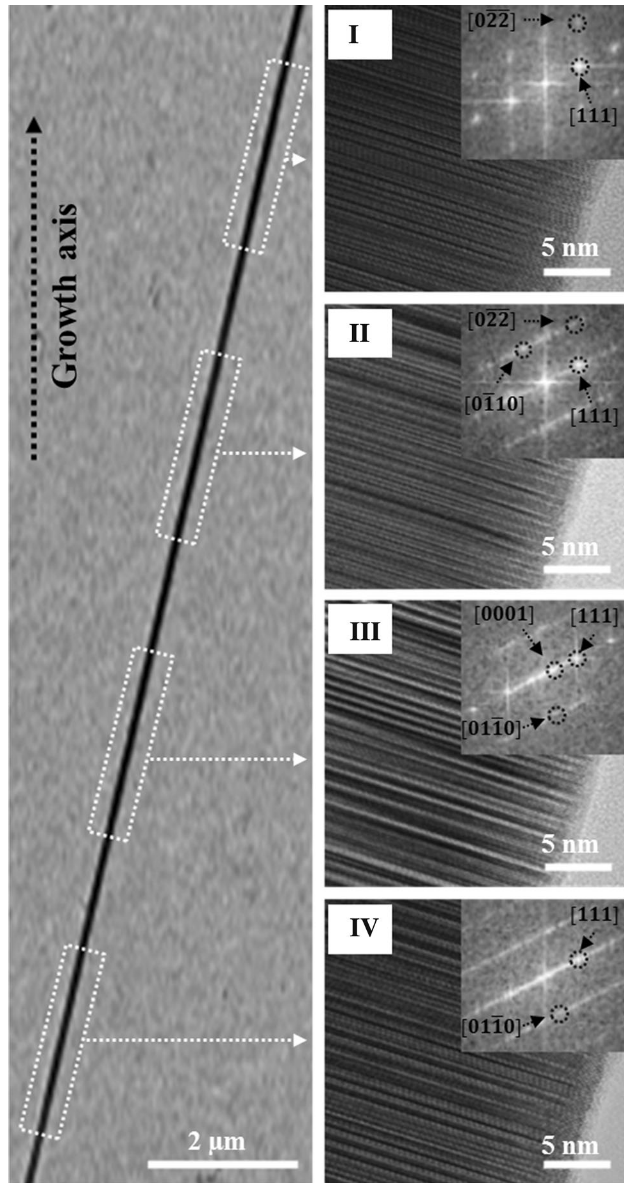

Fig. 2. Cs-TEM image (left) for an undoped InAs NW, the HRTEM images (right), and diffraction patterns (inset), measured at four different vertical positions of the InAs NW.

fields that lead to depletion of the NW surface, disturbing carrier moment. Similarly, the additional internal electric field due to the existence of more WZ structure in "Region-A" partly interferes with the carrier movement inside the InAs NW, leading to an increase in the resistance.

The electrical properties of the InAs NW depending on the crystal structures were additionally explored by applying gate bias. Figure 4a shows the transfer characteristic curves of InAs NW FET, measured at RT. The inset is a schematic diagram of the catalyst-free and undoped NW FET with a back gate. Compared to "Region-A", the device performance was significantly improved at "Region-B" with more ZB structure. More specifically, the field-

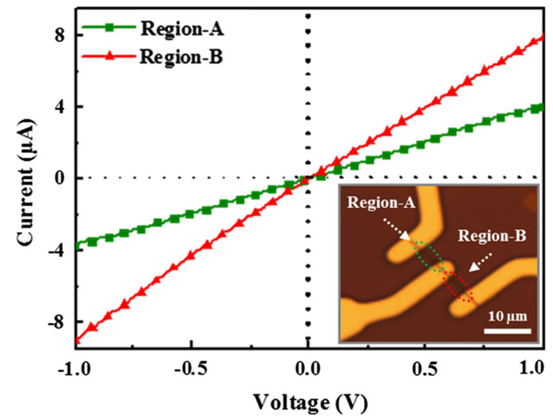

Fig. 3. I–V characteristic curves measured at the bottom (Region-A) and top (Region-B) areas of an InAs NW. Inset an OM image of an InAs NW with three electrodes.

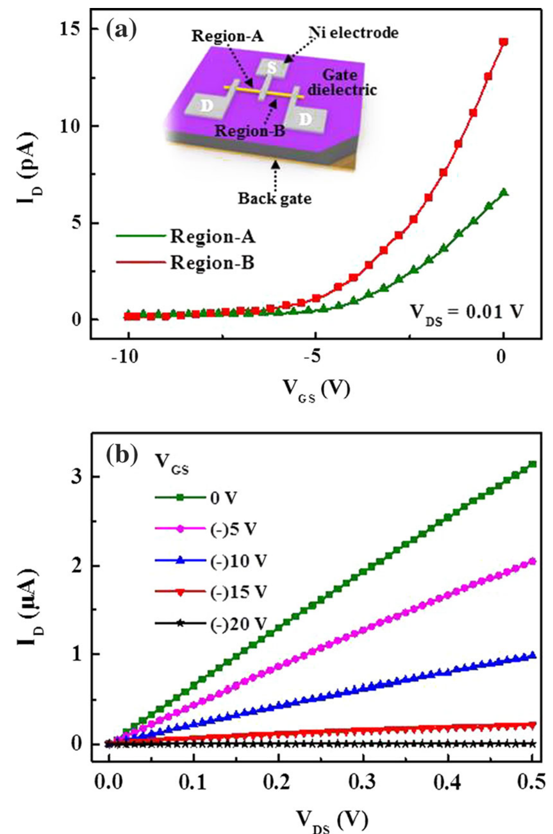

Fig. 4. (a) Transfer and (b) I_D–V_{DS} characteristic curves of a FET with an InAs NW. Inset a schematic structure of the FET with an InAs NW channel.

effect mobility increases from 507 to 1099 cm^2/V s. The on/off current ratio ($\sim 10^3$) was improved by one order of magnitude, which is also larger than those of previous works.[7,8] The increase in the mobility and on/off ratio is related to the reduction in the influence of the WZ structure and the stacking faults.[33,34] Figure 4b shows I_D–V_{DS} characteristic curves of the FET at various voltages of

V_{GS}, measured at RT. At a V_{GS} of 0 V, the I_D increases with increasing V_{DS}. In addition, the I_D–V_{DS} decreases by applying a negative V_{GS}. This indicates that the InAs NW channel for carriers is opened at the initial stage before applying an external bias and depleted with decreasing V_{GS}. As a result, the FET with an InAs channel is considered as a depletion type. There was no I_D flowing at the V_{GS} of − 20 V, because the InAs NW channel was completely depleted. In addition, it is noteworthy that the RT operation of the FET with an InAs NW having both ZB and WZ structures was successfully observed.

CONCLUSION

We investigated the positional effects of InAs NWs internal crystal structure with respect to their electrical properties. From the investigation of FE-SEM and Cs-TEM images, the WZ structure was predominantly observed with many stacking faults at the bottom region of the InAs NW. Vertically along the InAs NW, the number of WZ structures and the stacking faults reduced and the ZB structure was predominantly observed. Finally, the ZB crystal structure was dominant at the top region of the InAs NW. The resistance and resistivity of the top region of the InAs NW with the ZB structure were smaller than those of the bottom region with the WZ structure and had many stacking faults. The difference in the resistance and resistivity depending on the position of an InAs NW in the vertical direction is attributed to the amount of stacking faults and the degree of internal electric fields inherently caused by the WZ crystal structure. The I_D–V_{GS} and I_D–V_{DS} characteristic curves of the FET with an InAs NW as a channel were successfully obtained at RT.

ACKNOWLEDGEMENTS

This work was supported by the National Research Foundation of Korea (NRF) funded by the Ministry of Science, ICT and Future Planning (No. 2015042417) and by the Ministry of Education (No. 2015R1D1A1A01060681).

REFERENCES

1. A.C. Ford, J.C. Ho, Y.L. Chueh, Y.C. Tseng, Z. Fan, J. Guo, H. Bokor, and A. Javey, *Nano Lett.* 9, 360 (2009).
2. P. Offermans, M. Crego-Calama, and S.H. Brongersma, *Nano Lett.* 10, 2412 (2010).
3. S. Chuang, Q. Gao, R. Kapadia, A.C. Ford, J. Guo, and A. Javey, *Nano Lett.* 13, 555 (2013).
4. D. Yao, G. Zhang, and B. Li, *Nano Lett.* 8, 4557 (2008).
5. D.W. Park, S.G. Jeon, C.R. Lee, S.J. Lee, J.Y. Song, J.O. Kim, S.K. Noh, J.Y. Leem, and J.S. Kim, *Sci. Rep.* 10, 16652 (2015).
6. J. Hwang, B.K. Kim, S.J. Lee, M.H. Bea, and J.C. Shin, *Cur. Appl. Phys.* 15, S35 (2015).
7. S.A. Dayeh, D.P.R. Aplin, X. Zhou, P.K.L. Yu, E.T. Yu, and D. Wang, *Small* 3, 326 (2007).
8. S.A. Dayeh, D. Susac, K.L. Kavanagh, E.T. Yu, and D. Wang, *Adv. Funct. Mater.* 19, 2102 (2009).
9. G.K. Reeves and H.B. Harrison, *IEEE Electron Device Lett.* 3, 111 (1982).
10. S. Hertenberger, D. Rudolph, M. Bichler, J.J. Finley, G. Abstreiter, and G. Koblmüller, *J. Appl. Phys.* 108, 114316 (2010).
11. Y. Wang, V. Schmidt, S. Senz, and U. Goesele, *Nat. Nanotechnol.* 1, 186 (2006).
12. C. Thelander, P. Caroff, S. Plissard, A.W. Dey, and K.A. Dick, *Nano Lett.* 11, 2424 (2011).
13. J.V. Knutsson, S. Lehmann, M. Hjort, P. Reinke, E. Lundgren, K.A. Dick, R. Timm, A. Mikkelsen, and A.C.S. Appl, *Mater. Interfaces* 7, 5748 (2015).
14. V. Schmidt, J.V. Wittemann, S. Senz, and U. Gösele, *Adv. Mater.* 21, 2681 (2009).
15. K. Tomioka, J. Motohisa, S. Hara, and T. Fukui, *Nano Lett.* 8, 3475 (2008).
16. T. Tanaka, K. Tomioka, S. Hara, J. Motohisa, E. Sano, and T. Fukui, *Appl. Phys. Express* 3, 025003 (2010).
17. S. Hertenberger, D. Rudolph, S. Bolte, M. Döblinger, M. Bichler, D. Spirkoska, J.J. Finley, G. Abstreiter, and G. Koblmüller, *Appl. Phys. Lett.* 98, 123114 (2011).
18. B. Mandl, J. Stangl, E. Hilner, A.A. Zakharov, K. Hillerich, A.W. Dey, L. Samuelson, G. Bauer, K. Deppert, and A. Mikkelsen, *Nano Lett.* 10, 4443 (2010).
19. E. Dimakis, J. Lähnemann, U. Jahn, S. Breuer, M. Hilse, L. Geelhaar, and H. Riechert, *Cryst. Growth Des.* 11, 4001 (2011).
20. J. Miao, W. Hu, N. Guo, Z. Lu, X. Zou, L. Liao, S. Shi, P. Chen, Z. Fan, J.C. Ho, T.X. Li, X.S. Chen, and W. Lu, *ACS Nano* 8, 3628 (2014).
21. Z. Cuil, R. Perumal, T. Ishikura, K. Konishi, K. Yoh, and J. Motohisa, *Appl. Phys. Express* 7, 085001 (2014).
22. M. Fu, D. Pan, Y. Yang, T. Shi, Z. Zhang, J. Zhao, H.Q. Xu, and Q. Chen, *Appl. Phys. Lett.* 105, 143101 (2014).
23. A. Konar, J. Mathew, K. Nayak, M. Bajaj, R.K. Pandey, S. Dhara, K.V.R.M. Murali, and M.M. Deshmukh, *Nano Lett.* 15, 1684 (2015).
24. D.W. Park, Y.B. Ji, H. Hwang, C.R. Lee, S.J. Lee, J.O. Kim, S.K. Noh, S.J. Oh, S.H. Kim, T.I. Jeon, K.I. Jeong, and J.S. Kim, *Sci. Rep.* 6, 36094 (2016).
25. T. Akiyama, K. Sano, K. Nakamura, and T. Ito, *Jpn. J. Appl. Phys.* 45, L275 (2006).
26. M. Noguchi, K. Hirakawa, and T. Ikoma, *Phys. Rev. Lett.* 66, 2243 (1991).
27. D. Spirkoska, J. Arbiol, A. Gustafsson, S. Conesa-Boj, F. Glas, I. Zardo, M. Heigoldt, M.H. Gass, A.L. Bleloch, S. Estrade, M. Kaniber, J. Rossler, F. Peiro, J.R. Morante, G. Abstreiter, L. Samuelson, and A.F. i Morral, *Phys. Rev. B* 80, 245325 (2009).
28. D. Pan, M. Fu, X. Yu, X. Wang, L. Zhu, S. Nie, S. Wang, Q. Chen, P. Xiong, S.V. Molnár, and J. Zhao, *Nano Lett.* 14, 1214 (2014).
29. F. Zhou, A.L. Moore, J. Bolinsson, A. Persson, L. Fröberg, M.T. Pettes, H. Kong, L. Rabenberg, P. Caroff, D.A. Stewart, N. Mingo, K.A. Dick, L. Samuelson, H. Linke, and L. Shi, *Phys. Rev. B* 83, 205416 (2011).
30. Y.L. Chueh, A.C. Ford, J.C. Ho, Z.A. Jacobson, Z. Fan, C.Y. Chen, L.J. Chou, and A. Javey, *Nano Lett.* 8, 4528 (2008).
31. A.C. Ford, C.W. Yeung, S. Chuang, H.S. Kim, E. Plis, S. Krishna, C. Hu, and A. Javey, *Appl. Phys. Lett.* 98, 113105 (2011).
32. M.D. Schroer and J.R. Petta, *Nano Lett.* 10, 1618 (2010).
33. M. Fu, Z. Tang, X. Li, Z. Ning, D. Pan, J. Zhao, X. Wei, and Q. Chen, *Nano Lett.* 16, 2478 (2016).
34. C. Thelander, K.A. Dick, M.T. Borgström, L.E. Fröberg, P. Caroff, H.A. Nilsson, and L. Samuelson, *Nanotechnology* 21, 205703 (2010).